RESEARCH AND ANALYSIS ON THE OPERATING PERFORMANCE OF RIDGE ROLLERS UNDER DIFFERENT OPERATING MODES
/
起垄机不同作业模式下作业性能研究与分析

Xin ZHANG[1)], Yucheng LIANG[1*)], Lu GAN[1)], Yanliang ZHANG[1)], Yiwen YUAN[2)]
[1)] Heilongjiang Academy of Agricultural Machinery Engineering Sciences, Harbin 150081, China
[2)] College of Mechanical and Electrical Engineering, Heilongjiang University, Harbin, 150080, China
Tel: +86-18249059533; E-mail: xinzhang135689@163.com
DOI: https://doi.org/10.35633/inmateh-79-17

Keywords: *ridge roller, operating mode, resistance, ridge formation, experiment*

ABSTRACT
To explore the operational performance of a ridge roller under two different working modes, namely, linear arrangement (LA) and interleaved arrangement (IA) of adjacent ridging shovels, firstly, theoretical analysis was conducted to conclude that the operational resistance of IA is greater than that of LA. Secondly, a discrete element simulation method was employed to establish a discrete element simulation model. The extracted data verified the conclusions of the theoretical analysis. Qualitative analysis was conducted based on the formed ridge profile, indicating that LA has a better ridge forming effect than IA. Finally, field experiments were conducted, with the operating speed of the ridge roller (1.5 km/h, 3 km/h, 4.5 km/h) and different installation distances between adjacent ridging shovels (0, 240 mm, 480 mm) as experimental factors. The average operational resistance, the distance between adjacent ridge tops, and the height difference at the bottom of the ridge furrow were used as indicators for a full-factor experiment. It was concluded that under the same conditions, LA has the best ridge forming effect but requires the greatest resistance, while IA can effectively reduce resistance but has a poorer ridge forming effect. This study provides a theoretical basis and guidance for tillage and soil preparation operations.

摘要
为探究起垄机两种不同作业模式，即相邻起垄铲直线排布（LA）和交错排布（IA）下的作业性能，首先通过理论分析得出 IA 的作业阻力大于 LA；其次采用离散元仿真模拟方法，建立离散元仿真模型，通过提取数据验证了理论分析的结论，并通过形成的垄体断面轮廓进行定性分析，得出 LA 的垄体成型效果优于 IA；最后通过田间试验，以起垄机作业速度（1.5 km/h、3 km/h、4.5 km/h）和相邻起垄铲不同前后安装距离（0、240 mm、480 mm）为试验因素，以平均作业阻力和相邻垄体垄顶距离和垄沟最底端高度差为指标进行全因素试验，得出其他条件相同情况下，LA 的垄体成型效果最好，但是所需阻力最大，IA 阻力能有效降低但是垄体成型效果较差。本研究可为耕整地作业过程提供一定的理论依据和指导作用。

INTRODUCTION
The Northeast region is China's foremost grain production base, predominantly utilizing the ridge tillage method. This approach facilitates increasing soil temperature, enhancing water infiltration, and creating an optimal environment for crop root growth *(Zhao et al., 2025; Zhang et al., 2022; Yuan et al., 2019).* Therefore, rotary tillage and ridging operations are crucial components of agricultural mechanized production *(Shen et al., 2020; Guan et al., 2021).*

A large amount of research has been conducted both domestically and internationally on the issues of operational resistance and ridge formation effectiveness during rotary tillage and ridging operations. Scholars from the Nanjing Research Institute of Agricultural Mechanization under the Ministry of Agriculture have designed a sweet potato double-row ridging machine. The plow body primarily serves the function of furrowing, with a large amount of backfill soil *(Wang et al., 2025).* Researchers from Hunan Agricultural University have designed a plow-rotating combined rapeseed ditching and ridging machine. Compared to traditional ridging machines, it significantly improves soil fallback and achieves better ridging results (*Bao et al., 2017*). Some foreign researchers have also conducted comparisons on the ditching performance and fuel consumption of different ditching implements (*Kumar Sahu et al., 2018*).

Researchers from Henan Agricultural University optimized key components of the tobacco ridger and conducted experiments, resulting in reduced operational resistance and better consistency in ridge formation *(Song et al., 2024; Chen et al., 2022).* Scientific researchers and others have developed hillside land-leveling machines, but their functions are relatively limited, and the ridging effect is poor *(Zheng et al., 2021).*

Overall, current research on the operational resistance and ridge formation effectiveness of ridging machines primarily revolves around optimizing key components, with almost no theoretical research conducted on the most basic operational modes. Therefore, this paper focuses on two different operational modes of ridging machines, LA and IA, to study the factors affecting the operational resistance and ridge formation of ridging machines, aiming to provide theoretical support for rotary tillage and ridging operations.

MATERIALS AND METHODS

Ridge tiller operating mode

The ridger operates in two modes during its working process, and the top views of these two modes are illustrated in Fig. 1. The first mode involves the ridging shovels being aligned in a straight line. This ridging method ensures high uniformity and consistency in the ridges. However, on deeply plowed or rototilled soil, where there are numerous stems and stubble, and if the soil viscosity is high, the operational resistance increases, potentially leading to blockages and affecting the working efficiency, as depicted in Fig. 1(a). To address the blockage issue and reduce operational resistance, the second mode was developed, where adjacent ridging shovels are arranged in a staggered manner, maintaining a certain installation distance in the forward direction. This mode significantly reduces the likelihood of blockages, but it suffers from poor consistency in the shape of the ridges, as shown in Fig. 1(b).

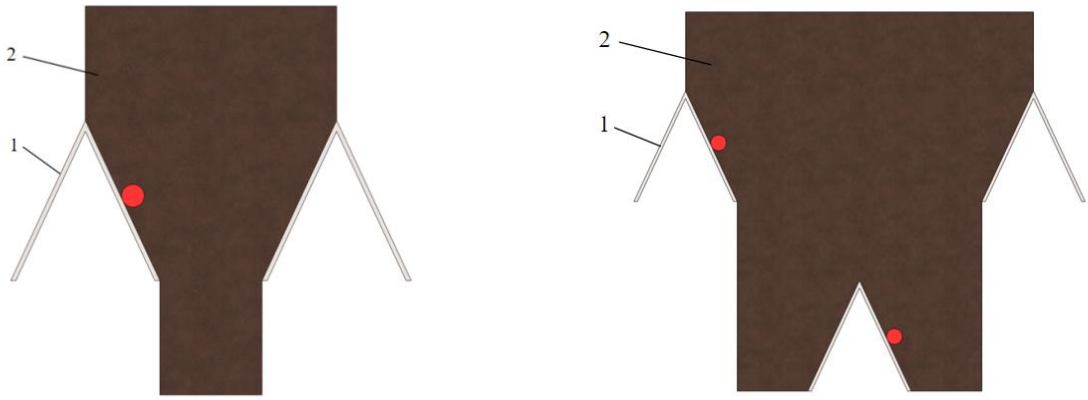

(a) Linear arrangement (LA) *(b) Interleaved arrangement (IA)*

Fig. 1 – Two ridge-forming modes
1. ridge shovel; 2. soil

Regardless of which operation mode the ridger adopts, the operation process will encounter significant resistance, requiring a power machine to provide substantial energy. To understand the force conditions on the ridging shovel under the two operation modes, a force analysis was conducted on one side plate of a single ridging shovel.

Force analysis of LA

When the ridging shovel is arranged in a straight line, the squeezing action between the inner plates of two adjacent ridging shovels will push the soil from a width of a_1 to a ridge width of b_1, thereby directly forming a ridge. At this time, the two side plates that help form the ridge platform are subjected to the force of the soil. In this operation mode, both sides of the ridge are squeezed by the side plates, and the soil can only move in a limited space, being completely constrained. In soil mechanics, this situation is referred to as the presence of infinite soil complete constraint on both sides of the ridge, assuming that the soil has a low moisture content or is dry and loose soil. A force analysis is conducted on any mass point O with a depth of h embedded in the soil on the side plate as it moves forward at a constant speed, as shown in Fig. 2.

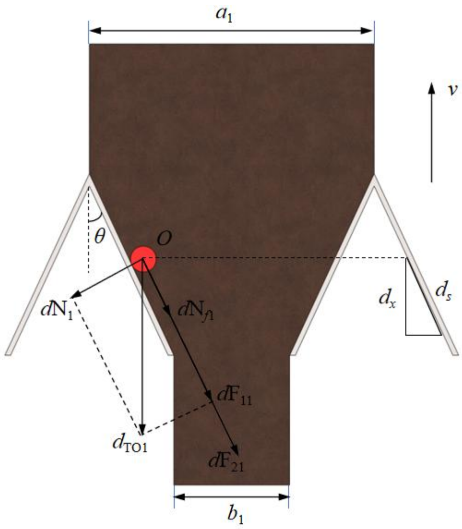

Fig. 2 – Force analysis of LA

In the figure, v represents the advancing direction of the ridging shovel, θ denotes the half-apex angle of the ridging shovel, dx signifies the displacement of particle O along the advancing direction, and ds indicates the displacement of particle O along the side plate. Calculations are performed based on Rankine's theory and assuming uniform normal pressure distribution on the side plate *(Waldron L.J., 1977*; *Waldron L.J. et al., 1981).*

$$\begin{cases} dA = hds \\ ds = \dfrac{dx}{\cos\theta} \\ dN_1 = pdA \\ dN_{f1} = \mu dN_1 \\ dF_{11} = \dfrac{dN_1}{\tan\theta} \\ dF_{21} = dN_{f1} + dF_{11} \\ p_1 = \xi\left(K_p\gamma h + 2c\sqrt{K_p}\right) \\ K_p = \dfrac{1+\sin\phi}{1-\sin\phi} \\ \xi = 1 + \left(K_p - 1\right)\dfrac{\tan\theta}{\tan\phi} \end{cases} \tag{1}$$

where:

dA—when the displacement in the forward direction is x, the area swept by the side plate in a small unit, m^2;

dN_1—normal pressure acting on a micro-unit area, N;

p_1—normal pressure per unit area, N;

dN_{f1}—friction force, N;

μ—coefficient of friction;

d_{F11}—the component of the total resistance of soil to the side plate in the direction of the side plate, N；

d_{F21}—total resistance in the direction of the side plate, N;

K_p—soil resistance coefficient under the condition of complete constraint on both sides of the side plate;

γ—soil bulk density;

β—the angle between the soil failure surface and the horizontal plane, (°) ;

Φ—Soil internal friction angle, (°);

c—Soil cohesion, typically ranging from 5 to 100 kPa for cohesive soil;

ξ—For the three-dimensional shape factor, when there is complete constraint from infinite soil on both sides of the ridge, based on Coulomb's passive earth pressure theory, this parameter needs to be introduced for three-dimensional correction.

By processing Eq. (1), the total drag force of the micro-unit in the direction of the side plate is obtained:

$$dF_{21}=\left[1+\left(\frac{1+\sin\phi}{1-\sin\phi}-1\right)\frac{\tan\theta}{\tan\phi}\right]\left[\frac{1+\sin\phi}{1-\sin\phi}\gamma h^2+2hc\sqrt{\frac{1+\sin\phi}{1-\sin\phi}}\right]\left(\mu\frac{dx}{\cos\theta}+\frac{dx}{\sin\theta}\right) \tag{2}$$

Force analysis of IA

When the ridging shovels are arranged in a staggered manner, during operation, the two adjacent ridging shovels at the front will first extrude soil from a width of a_2 to a ridge width of b_2, forming a large ridge. Subsequently, the middle ridging shovel located behind them will divide the ridge width b_2 into two ridges with a width of c_2. Unlike the analysis in the previous section, when two ridges with a width of c_2 are formed, there are no other ridging shovels on either side of the rear ridging shovel to press against its side plates. The two sides of the formed ridge are in free constraints, which is referred to as the absence of infinite soil body complete constraints on both sides of the ridge. A force analysis is conducted on any mass point O with a depth of h into the soil on the side plate, as shown in Fig. 3.

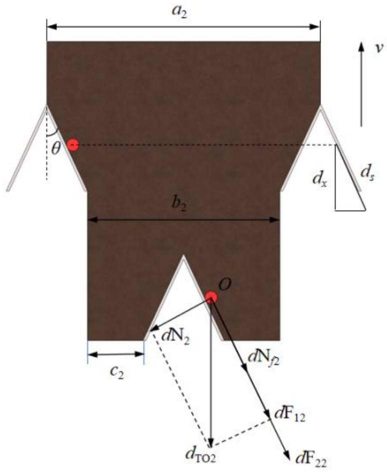

Fig. 3 – Force analysis of IA

Similar to the analysis in the previous section, there are:

$$\begin{cases} dA=hds \\ ds=\dfrac{dx}{\cos\theta} \\ dN_2=pdA \\ dN_{f2}=\mu dN_2 \\ dF_{12}=\dfrac{dN_2}{\tan\theta} \\ dF_{22}=dN_{f2}+dF_{12} \\ p=K_f\gamma h \\ K_f=\dfrac{\tan\beta+\cot(\beta+\theta)}{\tan\beta+\cot(\beta+\theta+\delta)}\dfrac{\sin\beta}{\sin\theta}\cos(\beta+\theta+\delta) \end{cases} \tag{3}$$

where: dN_2—normal pressure acting on a micro-unit area, N;

P_1—normal pressure per unit area, N;

dN_{f2}—friction force, N;

d_{F12}—the component of the total resistance of soil to the side plate in the direction of the side plate, N;

d_{F22}—total resistance in the direction of the side plate, N;

K_f—Soil resistance coefficient under free constraints on both sides of the side plate;

δ—The friction angle between the side plate and the soil, (°) .

By processing Eq. (2), the total drag force of the micro-unit in the direction of the side plate is obtained:

$$dF_{22} = \frac{\tan\beta + \cot(\beta+\theta)}{\tan\beta + \cot(\beta+\theta+\delta)} \frac{\sin\beta}{\sin\theta} \cos(\beta+\theta+\delta)\gamma h^2 \left(\mu \frac{dx}{\cos\theta} + \frac{dx}{\sin\theta} \right) \tag{4}$$

Based on the above analysis, it can be concluded that when the ridger operates in two different modes, the force conditions on the ridging shovel are completely different. When the friction force on the side plate of the ridging shovel is large, the corresponding power consumption of the entire machine is also high, and the wear on the side plate is also faster. Therefore, in order to reduce fuel consumption and extend the service life of the side plate of the ridging shovel, discrete element simulation analysis is conducted on the ridging shovel under the two operating modes, with the aim of qualitatively analyzing the force conditions on the ridging shovel and the consistency of the ridges in the two operating modes.

Ridge roller model establishment

The agricultural practice for corn cultivation in Northeast China primarily involves standard ridges with a ridge spacing of 650 mm. Therefore, the ridge spacing of the ridge roller model used in the simulation is set to 650 mm. To more clearly observe the simulated resistance of the two ridge-forming operation modes, the number of ridges is appropriately increased. Taking the example of forming four ridges with five ridge shovels, the simulation is conducted.

As the core component of the ridger, the ridging shovel bears almost all the operational resistance of the entire machine. Due to variations in ridging agronomic requirements across different regions, and considering only the differences in operational resistance of the ridging shovel under different arrangement modes and the consistency of ridge formation in this paper, the model is simplified. The digging shovel tip adopts a chisel-type tip and is installed at the bottom of the shovel handle using countersunk square root bolts. The soil divider plate is mounted on the lifting plate through a hinged shaft and can rotate at the hinged shaft to adjust the opening and closing angle. The three-dimensional diagram and key dimensions of the ridging shovel are shown in Fig. 4.

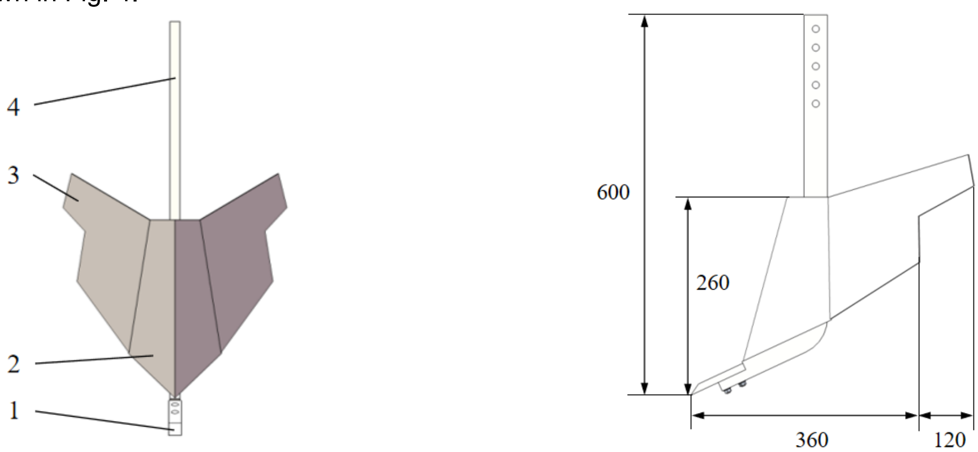

(a) Front view of ridging shovel
1.blade tip; 2.lifting board; 3.partition board; 4.shovel handle

(b) Side view of ridging shovel

Fig. 4 – Structural diagram of ridging shovel

During the simulation, based on agronomic requirements, the ridge top width is set at 250 mm. Using the 3D software SolidWorks 2020 (Dassault systems France, originally developed in USA), a model of the ridger is created according to the ridge forming conditions. The 3D models and key operational parameters of the ridger for two ridging modes are shown in Fig. 5. Since the ridge platform is formed by the contour created after the ridging process and subsequent compaction by the compaction wheel, this simulation analysis does not consider the factor of the compaction wheel. Therefore, the design specifies a distance of 200 mm between the ends of two adjacent soil divider plates (which is less than the top width of the ridge platform, which is 250 mm), a distance of 350 mm between the bottom ends of two soil divider plates, and a distance of 480 mm between the front and rear of two adjacent ridging shovels in the staggered arrangement mode.

(a) Top view of linear arrangement

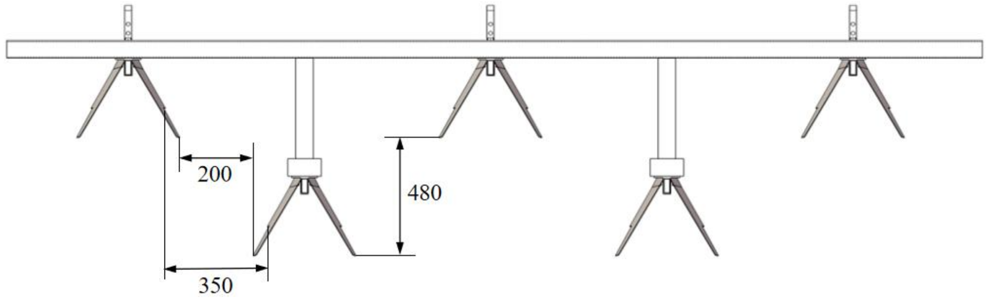

(b) Staggered arrangement top view

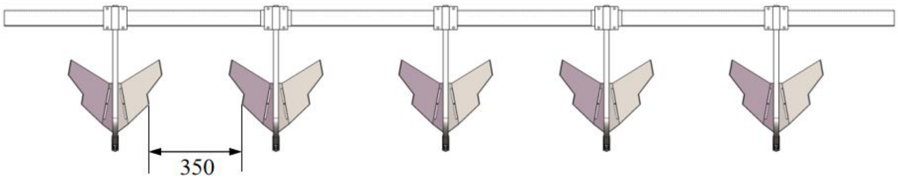

(c) rear view

Fig. 5 – Ridge roller operating mode

Establishment of discrete element simulation model

This study takes black soil in Northeast China as the research object. Based on the physical characteristics of Northeast black soil, a soil model is established using the discrete element software EDEM 2018 (USA). The simulation parameters are shown in Table 1 *(Zhao et al., 2021; Zeng et al., 2020; Ucgul M. et al., 2015; Zhang et al., 2023; Kojo A.et al., 2021; Hadi Z. et al., 2022)*.

Table 1

Parameters of Soil Model

Parameters	Values
Poisson's ratio	0.41
Shear modulus / MPa	1.24
Density / $(kg \cdot m^{-3})$	2150
Coefficient of restitution between soil particles	0.6
Static friction coefficient between soil particles	0.3
Rolling friction coefficient between soil particles	0.2
Normal contact bonding stiffness between soil particles / $(N \cdot m^{-3})$	3.4×10^8
Shear contact bonding stiffness between soil particles / $(N \cdot m^{-3})$	1.5×10^8
Critical normal stress / Pa	2×10^5
Critical shear stress / Pa	6.8×10^4
Bond radius / mm	5.5

Assuming that the field has undergone rotary tillage before ridging, resulting in fine and uniform soil, the external dimensions of the soil bin are determined based on the overall dimensions of the ridger, the ridging depth, the ridge-platform dimensions, and the ability of the ridger to form a distinct ridge in the simulation. Accordingly, the external dimensions of the soil bin are set to 3500 mm × 1500 mm × 300 mm (length × width × height). Due to the large volume of this soil bin, to shorten simulation time, the soil particle radius is set to 5 mm, and the soil particle generation type is selected with no limit on quantity, with a generation rate of 50,000 particles per second, and particle positions are randomly generated. The particles generated by the particle factory fill the soil bin under gravity. To make the bonding force between soil particles more consistent with field conditions, the soil bin is settled after being filled, and then continues to be filled until it is completely filled.

Save the overall model of the ridger in .stp format and import it into the EDEM soil bin model. The material is selected as 65 Mn, the depth of the ridging plate into the soil is 190 mm, and the forward speed is set to 3 km/h *(Liao et al., 2022)*. The simulation parameters of the ridger are shown in Table 2 *(Wang, 2019)*.

Table 2

Parameters of soil model

Parameters	Values
Poisson's ratio	0.3
Shear modulus / MPa	7.9×10^4
Density / ($kg\cdot m^{-3}$)	7865
Coefficient of restitution between the subsoiler and soil	0.6
Static friction coefficient between the subsoiler and soil	0.6
Rolling friction coefficient between the subsoiler and soil	0.05

The overall model under the two operating modes is shown in Fig. 6.

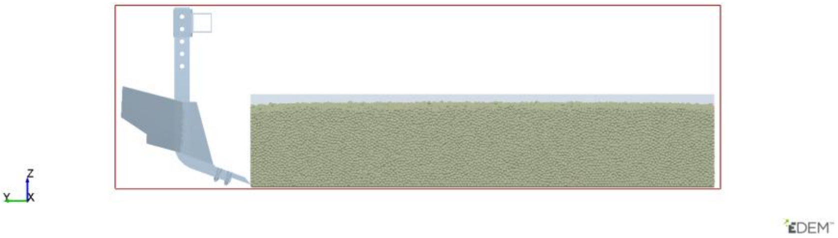

(a) Linear arrangement

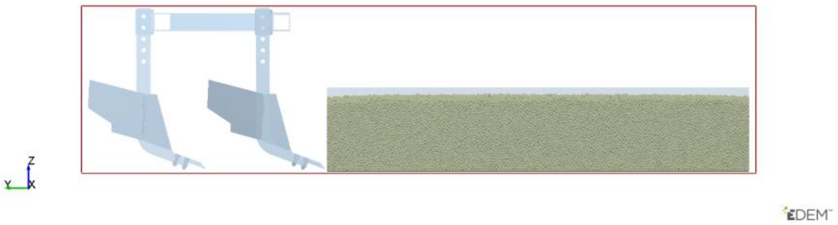

(b) Interleaved arrangement

Fig. 6 – Overall Model Construction

RESULTS

Simulation result of force analysis

The force and soil-velocity nephograms of the ridging shovel under the two operating modes of the ridger at the same time point are shown in Fig. 7.

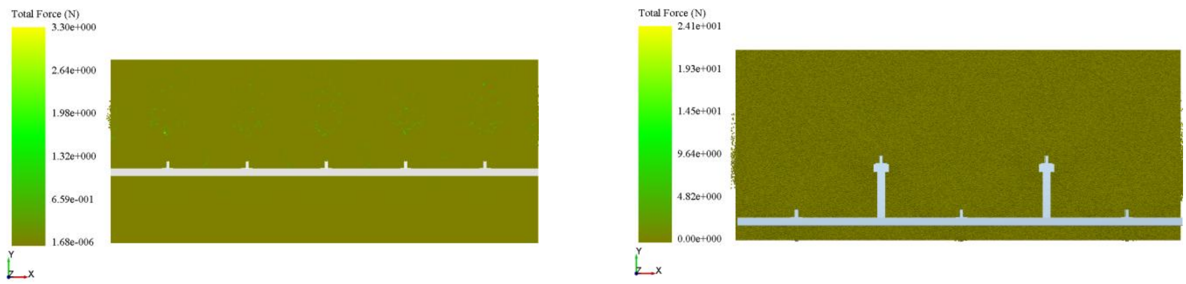

LA *IA*

(a) Ridge shovel force cloud map

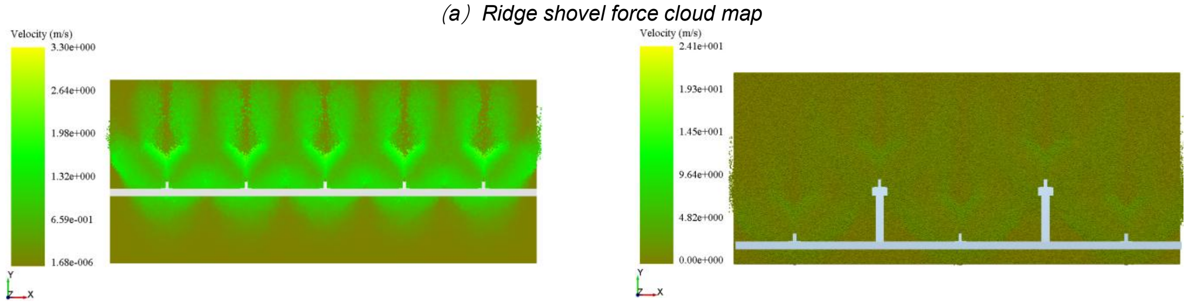

LA *IA*

(b) Soil velocity nephogram

Fig. 7 – Cloud Map Display

By extracting the force data at multiple identical time points after the ridging shovel is fully buried in soil under the two modes, and plotting the curves by Excel 2020, the results are shown in Fig. 8.

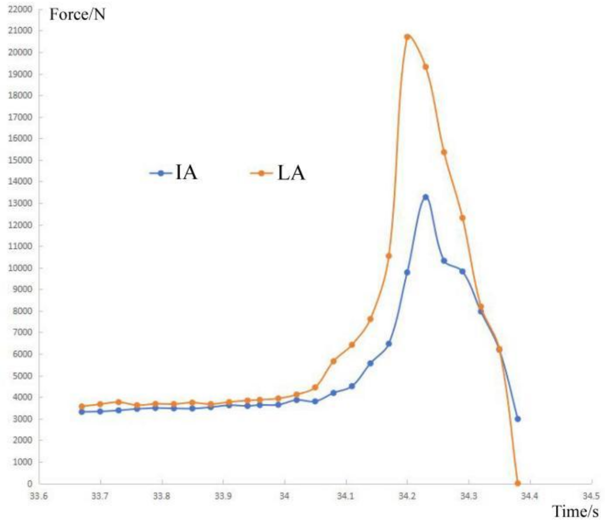

Fig. 8 – Force Line Graph of Ridging Shovel

Based on the analysis of the force cloud diagram and force polygonal line diagram of the ridging shovel, it can be concluded that the force exerted on the straight-line arrangement is greater than that on the staggered arrangement. According to the analysis of the soil particle velocity cloud diagram, the disturbance to soil particles caused by the straight-line arrangement is more pronounced than that caused by the staggered arrangement. This indicates that the closer the distance between two adjacent soil boards, the more pronounced the squeezing effect on soil particles during operation, and the greater the frictional force exerted on the adjacent soil boards. Consequently, the straight-line arrangement results in greater operational resistance and soil particle disturbance compared to the staggered arrangement.

Simulation result of ridge formation analysis

After the simulation of the ridging shovel is completed and the state of the soil particles in the soil bin has stabilized, cross-sections are taken at the same position on the ridge. The screenshots of the cross-sections under the two operating states are shown in Fig. 9.

（a）LA （b）IA

Fig. 9 – Cross-sectional View of the Ridge

Through observation and comparison, it can be seen that the shape of ridges formed by the straight arrangement is more consistent, with the depth of furrows being basically uniform. The bottom ends of the furrows are generally on the same straight line, and the distances l_1 and l_2 between the ridges of two adjacent ridges are basically consistent, as shown in Fig. 9(a). However, in the staggered arrangement, after the two ridging shovels located at the rear operate, the separated soil will move to both sides, causing soil to slide off the side of the ridge that is farther from the soil divider plate. This results in a height difference h_1 at the bottom end of the furrow, leading to poor consistency in the ridges, making the depth of the ridge platforms and furrows inconsistent, and there is a certain gap in the distance between the ridges of two adjacent ridges, with l_3 being slightly smaller than l_4, as shown in Fig. 9(b).

Based on the above analysis, it is preliminarily concluded that the linear arrangement mode results in greater resistance for the ridging machine but produces ridges with better consistency, while the staggered arrangement mode results in less resistance for the ridging machine but produces ridges with poorer consistency.

Field performance test

In the previous force analysis, it was conducted from a microscopic perspective, assuming low soil moisture content or dry soil, aiming to theoretically analyze the different forces exerted on the ridging shovel under two operating modes. According to relevant literature, the forward speed during operation also affects the force exerted on the ridging machine *(Tong et al., 2013; Jia et al., 2018).*

To explore the impact of different operating modes of the ridger on anti-blocking effect and ridge formation effect during actual operation, this chapter conducts a full-factor experiment based on the same structural parameters of the ridging shovel, using forward speed and the installation distance between adjacent ridging shovels as experimental factors, and taking operating resistance, the distance between the ridges of two adjacent ridges, and the height difference at the bottom of the furrow as indicators *(Wu, 2021).*

Test conditions and preparation

The field experiment was conducted at the experimental base of the Heilongjiang Academy of Agricultural Mechanization Engineering and Science in May 2025. The average stubble height of corn stalks was 103 mm, with soil hardnesses of 487 kPa (100 mm) and 1235 kPa (200 mm). The average soil moisture content was 16.2%, and the average root stubble moisture content was 38.6%. The experiment utilized a 1GZL-2 rotary tillage and ridging machine, which features rotary tilling at the front, three ridging shovels attached at the back, and an intermediate ridging shovel with an extension rod that allows for adjustment of the distance between adjacent shovels. This machine can form two ridges in a single operation. A photo of the rotary tillage and ridging machine is shown in Fig. 10.

Fig. 10 – Picture of rotary tillage and ridging machine

The equipment required for the experiment includes a Lovol 604 tractor (Shan dong, China), a GPS-10A multi-function testing device (Huade Soil Instrument Manufacturing Co., Ltd., Nanjing, China) for motor vehicles, a level ruler (Ningbo Deli Tools Co., Ltd., Zhejaing, China), a tape measure (Ningbo Deli Tools Co., Ltd., Zhejaing, China), a soil hardness meter (Huade Soil Instrument Manufacturing Co., Ltd., Nanjing, China), and a cutting ring assembly (Huade Soil Instrument Manufacturing Co., Ltd., Nanjing, China). The testing system is shown in Fig. 11.

Fig. 11 – Field experiment

The forward speeds were selected as 1.5 km/h, 3 km/h, and 4.5 km/h. As shown in Fig. 5(b), considering the front-to-rear dimension of the ridging shovel is 480 mm, the installation distances were chosen as 0, 240 mm, and 480 mm. To ensure a noticeable difference in resistance during each test, the forward distance for each test was set at 110 m, which includes a 10 m buffer zone and a 100 m effective working length. Each test was repeated three times. During the test, the forward speed was controlled by the tractor's electronic throttle, and the installation distance of the ridging shovel was adjusted by changing extension rods of different lengths. The coding of experimental factors is shown in Table 3.

Table 3

Experimental Factors and Levels

Level	Factors	
	Forward speed（km/h）	Front-to-rear installation distance（mm）
1	1.5	0
2	3	240
3	4.5	480

The operational resistance is represented by the average resistance within an effective operational length of 100 meters. The data acquisition method for the distance between the top of adjacent ridges and the height difference at the bottom of the furrow is as follows: within the experimental group corresponding to the effective operational length of 100 meters, three sets of data are randomly collected every 10 meters for recording.

The average operational resistance results are presented in Table 4.

Table 4

Analysis of Average Operational Resistance

Forward speed /（$km \cdot h^{-1}$）	Operating resistance of adjacent ridging shovels under different installation distances / N		
	0	240	480
	1542	1346	1295
1.5	1608	1377	1230
	1588	1285	1192
	1830	1602	1452
3	1857	1588	1389
	1760	1590	1490
	1944	1750	1633
4.5	2013	1681	1584
	2036	1684	1592

Analysis of the results in Table 4 reveals that when the forward speed remains constant, the operating resistance gradually decreases as the installation distance between adjacent ridging shovels increases. This trend aligns with the results of the theoretical analysis mentioned earlier, and the operating resistance is at its maximum when the installation distance between adjacent ridging shovels is zero. When the installation distance between adjacent ridging shovels remains constant, the operating resistance gradually increases as the forward speed increases.

The distance between the ridges of adjacent furrows is shown in Table 5.

Table 5

Distance Between the Tops of Adjacent Ridges

Forward speed /（$km \cdot h^{-1}$）	Distance between the ridges of adjacent furrows under different installation distances of adjacent ridge shovels / mm		
	0	240	480
	203	205	206
1.5	202	205	203
	203	204	206
	202	208	209
3	202	205	209
	201	207	208
	203	213	215
4.5	201	210	214
	203	211	217

Based on the analysis of the results in Table 5, it can be seen that when the forward speed remains constant, the distance between the ridges of adjacent furrows increases with the increase in the installation distance between adjacent furrowing shovels. When the installation distance between adjacent furrowing shovels is 0, the distance between the ridges of adjacent furrows is almost unaffected by speed. As the installation distance between adjacent furrowing shovels increases, the distance between the ridges of adjacent furrows is more significantly affected by speed, and the increase is more pronounced.

The height difference at the lowest end of adjacent ridges and furrows is presented in Table 6.

Table 6

Height difference at the lowest end of adjacent ridges and furrows

Forward speed / ($km \cdot h^{-1}$)	The height difference at the bottom of adjacent ridges and furrows under different installation distances between adjacent ridge shovels / mm		
	0	240	480
	3	8	9
1.5	2	8	8
	3	6	8
	2	10	15
3	1	11	18
	2	13	14
	4	17	30
4.5	3	20	41
	1	23	36

Based on the analysis of the results in Table 6, it can be seen that when the forward speed is constant, the height difference at the bottom of adjacent ridges and furrows increases with the increase of the installation distance between adjacent ridging shovels. When the installation distance between adjacent ridging shovels is 0, the height difference at the bottom of adjacent ridges and furrows is almost unaffected by speed. As the installation distance between adjacent ridging shovels increases, the height difference at the bottom of adjacent ridges and furrows is more significantly affected by speed, and the increase is more pronounced.

In all experimental groups, no blockage occurred, and it did not reach the level that required stopping the machine for cleaning. However, as the installation distance between adjacent ridging shovels increased, the accumulation of soil, straw, and stubble at the ridging shovel during operation was significantly alleviated.

CONCLUSIONS

(1) This article conducts a force analysis of the ridging shovel under two operating modes of the ridging machine (i.e., whether there is a front-to-back installation distance between two adjacent ridging shovels). Through theoretical analysis, it is concluded that the operating mode where the front-to-back installation distance between two adjacent ridging shovels is 0 results in a greater force on the ridging machine than the other mode.

(2) Using the discrete element simulation method, a discrete element model of the tiller-soil system was established. Under the condition of consistent other parameters, discrete element simulation tests were conducted for two operating modes with installation distances of 0 and 400 mm between adjacent tilling blades. This not only verified the previous conclusion, but also observed through the simulated ridges that the consistency of the ridges was also affected.

(3) A full-factorial field experiment was conducted, considering the forward speed of the ridger (1.5 km/h, 3 km/h, 4.5 km/h) and the installation distance between adjacent ridging shovels (0, 240 mm, 480 mm) as experimental factors. The experiment evaluated the ridger force, the distance between the ridges, and the height difference at the bottom of adjacent ridges as indicators. The results indicated that when the installation distance between adjacent ridging shovels was 0, the operational resistance was the highest, but the ridge formation effect was the best. As the forward speed and the installation distance between adjacent ridging shovels increased, the ridge formation effect gradually deteriorated. No blockage occurred during the experiment, but there was accumulation of soil, stems, and stubble at the ridging shovel, which could be effectively alleviated by increasing the installation distance between adjacent ridging shovels.

ACKNOWLEDGEMENT

This study was Supported by the Project of Laboratory of Advanced Agricultural Sciences, Heilongjiang Province (ZY04JD05-013); Heilongjiang province key research and development plan project (2024ZXDXB35) funding.

REFERENCES

[1] Bao, P., Wu, M., Guan, C., Luo, H., He, Y., Xiang, W., (2017). Design of plow-rotary style ditching and ridging device for rapeseed seeding (犁旋组合式油菜播种开沟起垄装置设计). *Transactions of the CSAE*, Vol. 33(20), pp. 23-31. China.

[2] Chen, X. (2022). *Design and Test of Successive Compaction Device of Tobacco Ridging, Fertilization and Compaction Machine (烟草起垄施肥机逐级压实装置设计与试验).* Zhengzhou: Henan Agricultural University. China.

[3] Guan, C., Cui, Z., Gao, Q., Wang, S., Chen, Y., Yang, Y., (2021). Design of biaxial rotary tillage soil test bench and layered tillage test (双轴旋耕碎土试验台设计与分层耕作试验). *Transactions of the CSAE*, Vol. 37(10), pp. 28-37. China.

[4] Hadi, A., Seyed, H., Mojtaba, N., (2022). Weed seed burial as affected by mouldboard design parameters, ploughing depth and speed: DEM simulations and experimental validation. *Biosystems Engineering*, Vol.216, pp.79-92. Iran.

[5] Jia H., Wang, W., Wang, W., Zheng, J., Wang, Q., Zhang, J., (2018). Application of anti-adhesion structure based on earthworm motion characteristics. *Soil & Tillage Research*, Vol.178, pp.159-166. China.

[6] Waldron L J., Dakessian S., (1981). Soil reinforcement by roots: calculation of increased soil shear strength from root properties. *Soil Science*, Vol.132(6), pp. 427-35. America.

[7] Kumar Sahu S., Tiwari K.B., Shrivastava P., (2018). Optimization of the kinematic parameter and fuel consumption for the side-shift offset rotavator using L and J-shape soil cutting blades. *International Journal of Current Microbiology and Applied Sciences,* Vol.7(8), pp. 1970-1982. India.

[8] Kojo, A., James, B., Diogenes, L., Antille, D., Mustafa, U., Troy, A., (2021). Analysis of effect of bent leg opener geometry on performance in cohesive soil using the discrete element method. *Biosystems Engineering*, Vol.209, pp.106-124. Ghana.

[9] Liao, Q., Du, W., Zhang, Q., Lin, J., Chen, Z., Zhang, J., (2022). Design and Experiment of Cigar Tobacco Adjustable Seed-plot Ridging and Film Spreading Machine (雪茄烟叶可调式苗床起垄铺膜机设计与试验). *Transactions of the Chinese society for agricultural machinery*, Vol.01, pp.1-13. China.

[10] Shen, H., Wang, B., Hu, L., Wang, G., Ji, L., Shen, G., Wu, T., (2020). Design of potato connecting and conveying mechanism for 4UZL-1 type sweet potato combine harvester device (4UZL-1 型甘薯联合收获机薯块交接输送机构设计). *Transactions of the CSAE*, Vol. 36(17), pp. 9-17. China.

[11] Song, Q. (2024). Design and Experiment of Compaction Device for Single-row Ridging Fertilizer Machine (单行起垄施肥作业机镇压装置设计与试验). Zhengzhou: Henan Agricultural University. China.

[12] Tong, J., Zhang, Q., Chen, D., Chang, Y., Wang, H., (2013). Effects of Bionic Geometric Structure Press Rollers on Reducing Rolling Resistance and Adhesion against Soil. *Applied Mechanics and Materials*, Vol.461, pp.63-72. China.

[13] Ucgul M., Fielke J M., Saunders C. (2015). Three dimensional discrete element modeling DEM of tillage accounting for soil cohesion and adhesion. *Biosystems Engineering*, Vol.129, pp. 298-306. Australia.

[14] Waldron L J. (1977). The Shear Resistance of Root-Permeated Homogeneous and Stratified Soil. *Soil Science Society of America Journal,* Vol. 41(5), pp. 843-9. America.

[15] Wang, B., Hu, L., Wang, S., Wang, B., Yu, Z., Wang, G., (2018). Design and Experiment of Sweet Potato Transplanting Operation Machine with Rotary Tillage, Ridging and Covering Film Functions (甘薯双垄旋耕起垄覆膜机的设计及试验研究). *Journal of China Agricultural University*, Vol. 23(7), pp. 116-125. China.

[16] Wang, J. (2019). *Design and Experiment of Subsoiler-stubble Chopper Device in No-tillage (免耕条件下破茬深松装置设计与 试验).* Harbin: Northeast Agricultural University. China.

[17] Wu, Y. (2021). *Design and experiment of an integrated machine for tobacco ridging, fertilizing and shaping (烟草起垄施肥整形一体机的设计与试验).* Zhengzhou: Henan Agricultural University. China.

[18] Yuan, T. (2019). *Experimental Study on Water-saving Effect of Summer Maize Under Ridge Tillage and Furrow Irrigation with Straw Mulching (秸秆覆盖条件下垄作沟灌夏玉米节水效应试验研究).* Zhengzhou: North China University of Water Resources and Electric Power. China.

[19] Zeng, Z., Ma, X., Chen, Y., Qi, L., (2020). Modelling residue incorporation of selected chisel ploughing tools using the discrete element method (DEM). *Soil and Tillage Research*, Vol.197, pp. 104505. China.

[20] Zhang, G., Yang, Y., Liu, Y., Wang, Z., (2022). Advances and Prospects of Soil Erosion Research in the Black Soil Region of Northeast China (东北黑土区土壤侵蚀研究进展与展望). *Journal of Soil and Water Conservation*, Vol. 36(02), pp. 1-12. China.
[21] Zhang, S., Zhao, H., Wang, X., Dong, J., Zhao, P., Yang, F., Chen, X., Liu, F., Huang, Y., (2023). Discrete element modeling and shear properties of the maize stubble-soil complex. *Computers and Electronics in Agriculture*, Vol.204:104579, China.
[22] Zhao, S., Liu, H., Yang, C., Yang, L., Gao, L., Yang, Y., (2021). Design and Discrete Element Simulation of Interactive Layered Subsoiler with Maize Straw Returned to Filed (玉米秸秆还田交互式分层深松铲设计与离散元仿真). *Transactions of the Chinese society for agricultural machinery*, Vol.52(3), pp.75-87. China.
[23] Zhao, S., Zhao, G., Leng， M., Liu, Z., Jiang, C., Yuan, Y., Yang, Y., (2025). Design and Testing of Serrated Stubble-breaking Blade with Interaction type with Subsoiler (与深松铲互作锯齿式灭茬刀设计与试验). *Transactions of the Chinese society for agricultural machinery*, Vol.56(04), pp.151-162. China.
[24] Zheng, Z., Fu, Z., Wang, C., (2021). Design and experimental research on soil covering device with linkage and differential adjustment of potato planter. *Agriculture,* Vol. 11, pp. 665. China.